PCCP

PAPER

Localized and delocalized bound states of the main isotopologue $^{48}O_3$ and of ^{18}O-enriched $^{50}O_3$ isotopomers of the ozone molecule near the dissociation threshold†

Cite this: DOI: 10.1039/d0cp02177f

Viatcheslav Kokoouline,*[a] David Lapierre,[b] Alexander Alijah[b] and Vladimir Tyuterev[bc]

Knowledge of highly excited rovibrational states of ozone isotopologues is of key importance for modelling the dynamics of exchange reactions, for understanding longstanding problems related to isotopic anomalies of the ozone formation, and for analyses of extra-sensitive laser spectral experiments currently in progress. This work is devoted to new theoretical study of high-energy states for the main isotopologue $^{48}O_3$ = $^{16}O^{16}O^{16}O$ and for the family of ^{18}O-enriched isotopomers $^{50}O_3$ = {$^{16}O^{16}O^{18}O$, $^{16}O^{18}O^{16}O$, $^{18}O^{16}O^{16}O$} of the ozone molecule considered using a full-symmetry approach. Energies and wave functions of bound states near the dissociation threshold are computed in hyperspherical coordinates accounting for the permutation symmetry of three identical nuclei in $^{48}O_3$ and of two identical nuclei in $^{50}O_3$, using the most accurate potential energy surface available now. The obtained vibrational band centers agree with observed ones with the root-mean-squares deviation of about 1 cm^{-1}, making the results appropriate for assignments and analyses of future experimental spectra. The levels delocalized between the three potential wells of ozone isomers are computed and analyzed. The states situated deep in the three (for $^{48}O_3$) or two (for $^{50}O_3$) equivalent potential wells have similar energies with negligible splitting. However, the states situated just below the potential barriers separating the wells, are split due to the tunneling between the wells resulting in the splitting of rovibrational sub-bands. We evaluate the amplitudes of the corresponding effects and consider possible perturbations in vibration–rotation bands due to interactions between three potential wells. Theoretical predictions for the splitting of observable band centers are provided for the first time.

Received 22nd April 2020,
Accepted 26th June 2020

DOI: 10.1039/d0cp02177f

rsc.li/pccp

1 Introduction

The ozone layer absorbs about 95% of the ultraviolet light from the Sun and is essential for the life on the Earth. For accurate monitoring of the layer and understanding its evolution, it is important to understand spectroscopic properties of O_3, mechanisms of its formation and destruction in the atmosphere, and its reactivity with other species present in the atmosphere.[1] The models used to interpret data from observations of the ozone layer are mainly based on experimental spectroscopic data.[2,3] *Ab initio* methods so far are unable to compete in accuracy with laboratory experiments in terms of transition frequencies, but theory helps to interpret complex laboratory spectra.[4] For example, theory is able to predict band energies and intensities[5–7] of radiative and, in some cases, collision-induced transitions. A significant part of vibration–rotation energies at the lower end of the ozone spectrum, below 8000 cm^{-1} above the ground vibrational level (ZPE), is relatively well known[5,8–16] (and references therein). For a reliable modelling and interpretation of ozone layer observations, knowledge of the higher-energy spectrum around the lowest O_2 + O dissociation limit, situated near 8500 cm^{-1} above the ZPE, is essential. The still lacking information on the corresponding levels and transitions is mandatory for the modelling of satellite measurements of the atmospheric ozone absorption and emission in the conditions of non-local thermodynamic-equilibrium.[2,17,18]

The spectroscopy of this energy region also plays an important role for understanding the dynamics of the formation and destruction of ozone. Despite many studies in this domain[19–23]

[a] *Department of Physics, University of Central Florida, Orlando, FL 32816, USA. E-mail: slavako@ucf.edu*
[b] *Groupe de Spectrometrie Moléculaire et Atmospherique, UMR CNRS 7331, University of Reims Champagne-Ardenne, F-51687, Reims Cedex 2, France. E-mail: alexander.alijah@univ-reims.fr, vladimir.tyuterev@univ-reims.fr*
[c] *Quamer Laboratory, Tomsk State University, Tomsk, Russia*

† Electronic supplementary information (ESI) available: Energies of band-centers and rotational constants. See DOI: 10.1039/d0cp02177f

(and references therein) one of the yet unsolved issues is the interpretation and theoretical modelling of isotopic anomalies[24–29] of the ozone formation that requires better knowledge of high energy states for the ozone isotopic species.

In this study, we predict and analyze highly-excited vibrational states of ozone isotopologues just below the lowest O_2 + O dissociation limit using an *ab initio* potential energy surface (PES) at a spectroscopic level of accuracy in a full symmetry approach.

The paper is organized in the following way. The next section outlines the theoretical methods used in the study. In Section 3, we discuss symmetry properties of the ^{18}O-enriched $^{50}O_3$ isotopomers of ozone, as well as energies and wave functions of deeply-bound and highly-excited delocalized vibrational levels. Section 4 is devoted to the main $^{48}O_3$ isotopologue, also using nuclear motion variational calculations in the three potential wells of the ozone PES. The results are compared with experimental data and with previous calculations. New features with respect to the one-potential-well approximation, which was traditionally employed in ozone spectroscopy, are discussed. Possible impacts of perturbations in observable vibration–rotation bands related to the interactions among potential wells are considered here for the first time. A full set of accurate vibrational energies and expectation values of rotational constants for each vibration level calculated in a global three-wells approach is provided as ESI.† Section 5 concludes the paper.

2 Theoretical method and potential energy surface

In this study, energies and wave functions of ozone bound states are obtained using a full symmetry approach in hyperspherical coordinates.[30–35] Technical aspects of the methods have been described in detail in our previous paper devoted to metastable ozone states and their life times[36] where the reader can find the corresponding definitions. For the sake of brevity in what follows, we shall distinguish the main ozone isotopologue $^{48}O_3$ = $^{16}O^{16}O^{16}O$ and the set of three ^{18}O-enriched isotopomers $^{50}O_3$ = $^{16}O^{16}O^{18}O/^{16}O^{18}O^{16}O/^{18}O^{16}O^{16}O$ by the total atomic mass given as left-hand upper case index. Calculations for rare ^{17}O-enriched species are not considered here and will be reported elsewhere.

The ozone molecule is known to possess a quite complicated electronic structure, which had been subject of many *ab initio* studies.[5,6,37–44] Due to the Jahn–Teller effect[45–47] the adiabatic electronic ground state of ozone has four minima.[38] Three identical minima, which are relevant to the present work, correspond to the lowest ''open'' geometrical configurations. They have locally C_{2v} symmetry forming isosceles equilibrium structures with two distances between oxygen atoms of 2.4095 Bohr and the third distance of 4.104 Bohr.[5] Three different arrangements of the oxygen atoms are thus placed in three identical potential wells separated by barriers. The $O_3 \rightarrow O_2 + O$ dissociation channels from each of these wells correspond to a D_0 threshold of about 1.05 eV $\approx$ 8500 cm^{-1} (in case of $^{48}O_3$). The fourth ''ring'' minimum[38] lies much higher – by about 1.34 eV – than the three open ones and is not relevant for ozone spectroscopy or dynamics in gas phase conditions.

Table 1 Symmetry species of the asymmetric top functions in $C_{2v}(M)$. e and o mean even and odd, respectively. In parentheses the classification according to Bunker and Jensen[62]

K_a	K_c	Γ
e	e	A_1
e	o	B_2 (B_1)
o	e	B_1 (B_2)
o	o	A_2

First large scale *ab initio* calculations of vibrational levels in the electronic ground state of ozone have been reported by Siebert *et al.*,[38,39] but the corresponding SSB potential energy surface (PES)[38] underestimated the dissociation threshold by 936 cm^{-1}, which represents more than 10% error in this quantity. It possessed an activation barrier at the transition state OO–O distance of about 4 Bohr, which was transformed into the so-called ''reef'' structure with increasing atomic basis set,[48] but this structure had not been confirmed later on by analyses of experimental spectra recorded with a highly sensitive laser cavity-ring-down spectrometer.[13,49] More elaborated electronic structure calculations by Dawes *et al.*[42] suggested that this reef should be converted to a smooth shoulder when using a larger space of orbitals. Their DLLJG PES[44] has been used in many recent studies.[50–54] Another *ab initio* PES, the TKTHS PES, has been constructed by Tyuterev *et al.*,[5] which accounts for the finding of Dawes *et al.*,[42] but used larger atomic basis sets with increasing cardinal number AV5Z $\rightarrow$ AV6Z $\rightarrow$ towards the complete basis set limit. This PES permitted to perform the to date most accurate *ab initio* spectra calculations in the range below 8000 cm^{-1}[4,6,12–15,49] (and references therein). Furthermore, it produced results in a good agreement with experiments for isotopic exchange reactions $^{16}O^{16}O + {}^{18}O \rightarrow {}^{50}O_3{}^* \rightarrow {}^{16}O + {}^{16}O^{18}O$,[55,56] where $^{50}O_3{}^*$ stands for the metastable ozone composed of two ^{16}O and one ^{18}O isotopes. The TKTHS[5] and DLLJG[44] PESs provide quite accurate theoretical estimations for the mass-independent value of the dissociation asymptote D_e(TKTHS) = 1.137 eV and D_e(DLLJG) = 1.150 eV. The first PES underestimates it by about 0.5% and the second one overestimates it by a similar percentage with respect to the latest experimental result D_e(exp) = 1.143 eV evaluated from thermochemical measurements by Ruscic *et al.*[57] (as cited by Holka *et al.*[41]). A comparison of key features of recent *ab initio* PESs of ozone with respect to experimental data including fundamental frequencies and dissociation energy can be found in Table 1 by Yuen *et al.*[56]

The present work aims at a detailed investigation of the bound states of $^{50}O_3$ and $^{48}O_3$ ozone isotopologues near the dissociation threshold. We focus here on the tunneling-type effects related to the delocalization of wave functions from the potential well above 8000 cm^{-1} and on their possible impact on observable vibration–rotation bands. To this end, an accurate

potential energy surface and global variational calculations in the three-wells are necessary. As in the previous work[36] we employ the spectroscopically accurate TKTHS PES[5] symmetrized with respect to the three potential wells of the ozone molecule. The solution of the nuclear motion equation is performed in two steps following the procedure described by Kokoouline *et al.*,[31–33] previously applied for H_3^+[35] and ozone metastable states.[36] First, one solves the equation in the space of the two hyperangles θ, ϕ with a fixed value of the hyperradius ρ. This produces hyperspherical adiabatic wave functions (adiabatic channels) and their energies (adiabatic curves). In the second step,[58] the hyper-radial Schrödinger equation is solved using the adiabatic functions as an expansion basis in the space of the hyperangles. In reality, the hyper-radius is not a good adiabatic coordinate. As a result, a relatively large number of adiabatic channels is required in the expansion to obtain satisfactory convergence. In present calculations, 210 adiabatic channels were used for the $^{16}O^{16}O^{18}O$ isotopologue and 160 channels for $^{48}O_3$. The number of basis functions along the hyper-radius was 192 for the both isotopologues. With these parameters, the uncertainty of the obtained energies with respect to the employed numerical method is approximately 0.01 cm^{-1} for $^{50}O_3$ and better than 0.01 cm^{-1} for $^{48}O_3$. In the following discussion, the energy origin is assumed to be at the energy of the lowest vibrational level of the considered isotopologue of the ozone ground state. Atomic masses of the two isotopes of Oxygen were used in the calculations.

3 ^{18}O-enriched isotopomers $^{16}O^{16}O^{18}O/^{16}O^{18}O^{16}O/^{18}O^{16}O^{16}O$

3.1 Symmetry considerations

For vibration–rotation states of the three $^{50}O_3$ isotopomers near the potential minima, only two wells are equivalent due to mass-dependent kinetic effects. They correspond to asymmetric arrangements ($^{16}O^{16}O^{18}O$ and $^{18}O^{16}O^{16}O$) of the heavy ^{18}O oxygen atom and will be denoted well-I and well-II. The well-III corresponds to symmetric arrangement $^{16}O^{18}O^{16}O$. The three potential minima are quite deep (about 1.14 eV from the bottom of the PES to the O_2 + O asymptote) so that the tunneling effect between vibrational levels in different minima is not measurable for low energy levels and, therefore, can be neglected. Neglecting the tunneling effect and using normal mode notations, the vibrational levels are characterized by the usual triad of quantum numbers (ν_1, ν_2, ν_3) of the symmetric stretching ν_1, bending ν_2, and anti-symmetric stretching ν_3 modes.

In most of previous works devoted to experimental spectra assignments[4,8,12,59–61] (and references therein) for energies deep in the potential wells, the asymmetric isotopomers are considered as identical ones (with abbreviated notation 668 = $^{16}O^{16}O^{18}O$ = $^{18}O^{16}O^{16}O$) and corresponding to the C_s point group. In this traditional approach, all vibrational levels of C_s isotopic species have A' symmetry type and are spin-allowed. For the 686 = $^{16}O^{18}O^{16}O$ isotopomers sitting deep in the potential well-III, the point group is C_{2v}. The symmetric stretching and bending vibrational modes are of the A_1 irreducible representation (irrep), whereas the anti-asymmetric stretching mode is of the B_1 irrep in the C_{2v} group in a standard choice of the molecular-fixed frame of x, y, z-axes usually adopted in spectroscopic works.[4,8] Only $J = 0$ states for even ν_3 quantum number are spin-allowed in this case.

Table 2 Allowed rovibrational states for the *XXY* and *XYX* type molecules formed from ^{16}O and ^{18}O

Γ_{rovib}	Γ_{vib}	Γ_{rot}	$J_{K_aK_c}$
Ψ^A_{XXY} or Ψ_{XYX}, ν_3 even			
A_1	A	A_1	J_{ee}
A_2	A	A_2	J_{oo}
Ψ^B_{XXY} or Ψ_{XYX}, ν_3 odd			
A_1	B	B_1	J_{oe}
A_2	B	B_2	J_{eo}

Here, in a global approach including the three wells for the family of isotopomers $^{50}O_3$ = $^{16}O^{16}O^{18}O/^{16}O^{18}O^{16}O/^{18}O^{16}O^{16}O$, we consider the full permutation-inversion symmetry group ($S_2 \times I = C_{2v}(M)$),[62] which contains the permutation operation (12) of two indistinguishable ^{16}O atoms, the inversion operation E^* and their product. To characterise vibrational functions, which are invariant under inversion E^*, it will be sufficient to use the sub-group S_2. They belong to two types, A and B, corresponding to the symmetry (irreps) of the functions with respect to the operator (12) of permutation of the identical atoms:

$$(12)|\nu,A\rangle = |\nu,A\rangle,\ (12)|\nu,B\rangle = -|\nu,B\rangle. \quad (1)$$

In the discussion below, the notation $|\nu\rangle$ will be replaced with $|\nu_1,\nu_2,\nu_3\rangle$ when approximate quantum numbers of the normal modes should be specified explicitly.

3.2 Vibration–rotation levels, wave functions and bands

Vibration–rotation bound state wave functions can be expanded in the basis set formed as a direct product of vibrational and rotational functions

$$\psi^{J\Gamma}_{vib-rot} = |\nu\rangle|JK_aK_c\rangle + \sum_{\nu' K_a' K_c'} |\nu'\rangle|JK_a' K_c'\rangle, \quad (2)$$

where the first term corresponds to a dominant contribution, which is typically used for spectroscopic assignment of the corresponding levels $E^{\Gamma}_{\nu JK_aK_c}$. Here $|\nu\rangle$ is an eigen-function of the vibrational Hamiltonian, which in our case is given by eqn (8) of ref. 36. It is computed in hyperspherical coordinates as described in Section III of our previous paper[36] for the main $^{48}O_3$ isotopologue. The computational technique for $^{50}O_3$ is quite similar, with the corresponding changes of masses in the kinetic part of the Hamiltonian. J is the total angular moment and Γ is the irreducible representation (irrep) of the full permutation-inversion $C_{2v}(M)$ symmetry group of $^{50}O_3$. Because the principal moments of inertia at each potential minimum are different, the standard asymmetric top functions $|JK_a'K_c'\rangle$ can be used as a rotational basis set[63] in eqn (2), where the axes

a and b of principal moment of inertia are in the molecular plane, while the c-axis is perpendicular to the plane. The symmetry species of the asymmetric top functions in the permutation-inversion group $C_{2v}(M)$ are given in Table 1.

Note that A and B are the characters with respect to (12), and the subscripts 1 and 2 denote positive or negative parity (inversion operator E). The ^{16}O and ^{18}O nuclei are bosons with zero spin. Consequently, the spin weights of A_1 and A_2 rovibrational states is equal to 1, whereas the spin weights of B_1 and B_2 rovibrational states is zero. The spin-allowed rovibrational states of $^{50}O_3$ isotopomers are collected in Table 2. Table 2 applies to both the *XXY* molecule and the *XYX* molecule, where $|\Psi_{XYX}\rangle = |\nu_1\nu_2\nu_3\rangle_{III}$ transforms as A_1 for ν_3 even and as B_1 for ν_3 odd.

Knowledge of vibration–rotation levels permits calculating positions of observable transitions

$$E^{\Gamma'}_{\nu' J' K_a' K_c'} \rightarrow E^{\Gamma}_{\nu J K_a K_c} \tag{3}$$

of rovibrational bands in experimental spectra. One of the key parameters for an assignment of observed spectra is the center of a rovibrational band, which is experimentally determined by following J-dependent series of lines towards the $J \rightarrow 0$ limit. Theoretically, the band center can be easily computed from the upper state level which is the eigen-value of the purely vibrational Hamiltonian. For the $J = 0$ levels of $\Gamma_{vib} = A$ the spin weight is equal to 1 whereas for the $J = 0$ levels of $\Gamma_{vib} = B$ the spin weight is equal to 0. In the latter case the corresponding pure vibrational states are missing, but rovibrational bands associated with these vibrations do exist. Thus, knowledge of both $E^{A}_{\nu J=0}$ and $E^{B}_{\nu J=0}$ vibrational levels is necessary for theoretical predictions of the corresponding band centers. Note that this was also the case in the framework of the traditional one-well approach.[4,6,8,11] The vibrational functions $|\nu\rangle$ do exist for both symmetry types as factors in the dominant contributions of the rovibrational wave functions (2). The study of their shapes and nodal lines is useful for the corresponding band assignment.

We shall show in the following sections that interactions among the three ozone potential wells result in perturbations of rovibrational bands near the dissociation threshold *via* A/B splitting of sub-band centers and due to changes in rotation energy patterns.

3.3 Levels localized in potential wells of ^{18}O enriched isotopomers

Let us first consider "cold" bands (3) corresponding to transitions from the ground vibrational state $\nu' = 0$, which are the strongest ones in the atmospheric conditions. For symmetric isotopomers 686 = $^{16}O^{18}O^{16}O$ localized in the potential well-III, there exist two types of bands. In the so-called "parallel" bands (due to the dipole moment component, which is parallel to the a-axis of the principal moment of inertia) the observed transitions reach only (J, K_a = e, K_c = o) and (J, K_a = o, K_c = e) levels.[4,8] These bands correspond to odd $\Delta\nu_3$ values with the B-type vibrational upper state wave functions $|\nu B\rangle$ in the dominant contribution of eqn (2). The $J = 0$ upper state level $E^{B}_{\nu,J=0}$ has zero spin weight, but determines the corresponding band center.

In the "perpendicular" bands (due to the dipole moment component along b-axis, which is perpendicular to the a-axis of the principal moment of inertia) the observed transitions reach only (J, K_a = e, K_c = e) and (J, K_a = o, K_c = o) levels.[4,8] These bands correspond to even $\Delta\nu_3$ values with the A-type vibrational upper state wave functions $|\nu A\rangle$ in the dominant contribution of eqn (2). There is no degeneracy between $E^{A}_{\nu,J=0}$ and $E^{B}_{\nu,J=0}$ levels near the minimum of the symmetric well-III, and the centers of parallel and perpendicular bands of the 686 isotopomer are significantly separated. We shall denote the vibrational wave functions of $^{50}O_3$ localized in the symmetric 686 well-III as

$$\begin{aligned} |s;\nu,A\rangle &= |\nu,A\rangle_{III}, \\ |s;\nu,B\rangle &= |\nu,B\rangle_{III}, \end{aligned} \tag{4}$$

where symbol s stands for "symmetric arrangement". Labels A and B refer to the symmetry transformation with respect to the (12) permutation of identical ^{16}O nuclei. In the approximation usually adopted in ozone spectroscopy,[4,8] this isotopomer, localized in well-III, was considered as a separate species belonging to the C_{2v} point group. The selection rules for the 686 isotopomer are the same as in the spectra of the main ozone isotopologue $^{48}O_3$, for which *ab initio* vibration–rotation transitions were reported in ref. 6 and 7.

For asymmetric isotopomers 668 = $^{16}O^{16}O^{18}O/^{18}O^{16}O^{16}O$, localized in the potential well-I or well-II, we have to consider the following vibrational functions

$$\begin{aligned} |a;\nu,A\rangle &\sim \frac{1}{\sqrt{2}}(|\nu\rangle_I + |\nu\rangle_{II}), \\ |a;\nu,B\rangle &\sim \frac{1}{\sqrt{2}}(|\nu\rangle_I - |\nu\rangle_{II}), \end{aligned} \tag{5}$$

where symbol "a" stands for asymmetric arrangement of ^{18}O. The corresponding cold bands have similar selection rules in terms of K_a and K_c quantum numbers as the 686-bands of the same upper state vibrational symmetry. However, in contrast to the case of the 686 states of eqn (4), the vibrational levels $E^{A}_{\nu,J=0}$ and $E^{B}_{\nu,J=0}$ of wave function, given by eqn (5), are near-degenerate at the bottom of the potential wells. This gives rise to so-called "hybrid" rovibrational bands,[59–61] which are experimentally seen as composed of parallel and perpendicular sub-bands with the same sub-band centers. The existence of such hybrid bands of the 668 isomers at low energies was known and taken into account for spectra assignments in a framework of standard spectroscopic models using the one-well approximation.[4,8,11,59–61] In this latter approach, the $^{16}O^{16}O^{18}O/^{18}O^{16}O^{16}O$ species were considered as identical ones belonging to the C_s point group.

Our calculations accounting simultaneously for the three potential wells show that wave functions of all $^{50}O_3$ vibrational levels are strongly localized either in the symmetric ($^{16}O^{18}O^{16}O$) or asymmetric ($^{16}O^{16}O^{18}O/^{18}O^{16}O^{16}O$) wells for energies below approximately 8200 cm^{-1} (that is about 96% of the dissociation threshold D_0).

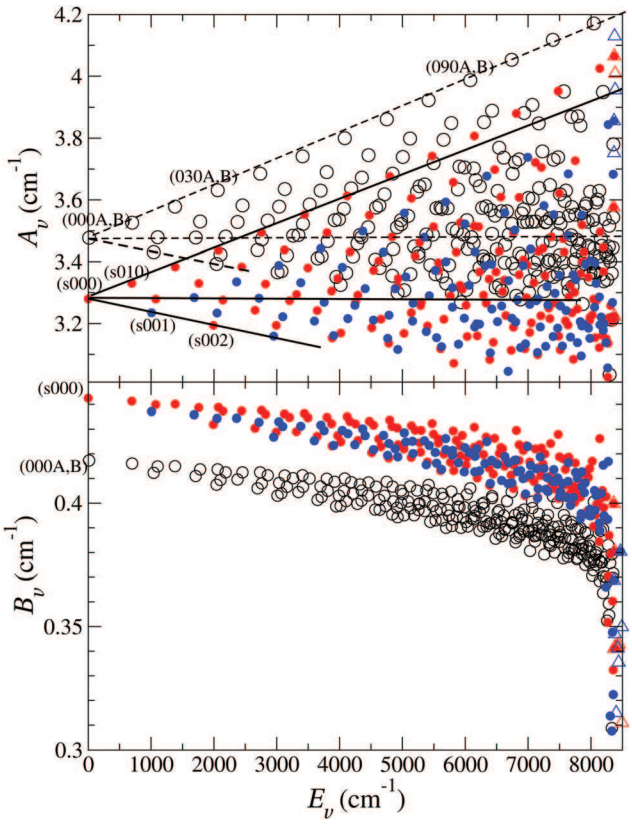

Fig. 1 Vibrational dependence of the rotational constants A_ν and B_ν of the $^{50}O_3$ bound levels. Open black circles show levels mainly localized in wells I and II. The A and B levels in these wells are quasi-degenerate below 8350 cm^{-1}. The red and blue solid circles show energies of A and B levels mainly localized in well III. These levels are not degenerate. The open red and blue triangles correspond to the levels above 8360 cm^{-1}, which are in general delocalized between the three wells.

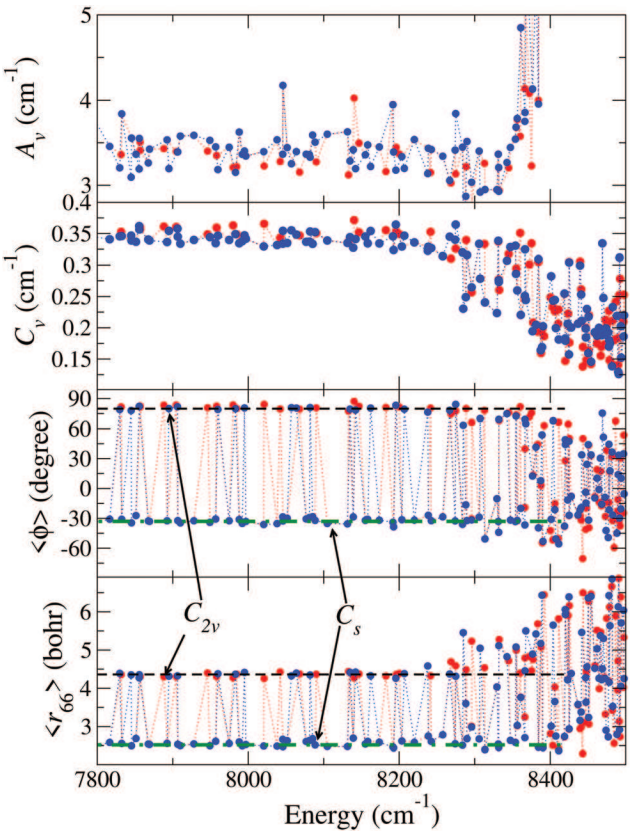

Fig. 2 Averaged values for several quantities of $^{50}O_3$ excited vibrational levels of the A (red symbols) and B (blue symbols) irreps. The upper panel and the one below show the largest, $\langle A_\nu \rangle$, and smallest, $\langle C_\nu \rangle$, of the three rotational constants, respectively. The third panel from the top gives the value of the cyclic hyperangle ϕ averaged in the interval $\phi \in [-\pi/2;\pi/2]$. The lowest panel shows the distance between the two ^{16}O atoms. The black horizontal dashed lines indicate values of $\langle \phi \rangle$ and $\langle r_{66} \rangle$ for levels situated deeply in the C_{2v} well, while the dashed-doted lines correspond to levels situated deeply in the C_s well.

Energies and expectation values of the two rotational constants A_ν and B_ν of the $^{50}O_3$ vibrational levels are shown in Fig. 1. From the A_ν constants (the upper panel of the figure), it is clear that there are several distinct families of vibrational levels. First, one distinguishes the levels mainly localized in the symmetric 686 well (open symbols in the figure) from the levels in the asymmetric 668 wells (closed symbols in the figure). The constants A_ν of the symmetric-well levels are, in general, smaller for the same combination of the ν_1, ν_2, ν_3 quantum numbers, than those of the levels in the asymmetric wells, due to a larger moment of inertia with respect to the a-axis.

The A and B levels, localized in the symmetric well, have different energies and are distinguished in the figure by red and blue closed symbols. In the asymmetric wells, energies of the A and B levels are almost degenerate, they are shown by open circles. The levels which are delocalized between the wells are marked with open red and blue triangles.

The figure also shows that the two families of localized levels are split in series of progressions, where only one quantum number of the normal modes changes at a time. These levels are labeled by the (ν_1, ν_2, ν_3) triad. Solid and dashed lines in the figure indicate some of the progressions in the symmetric 686 and asymmetric 668 wells, respectively, with wave functions of the type of eqn (4) and (5): The dashed and solid lines with increasing slopes show progressions of bending-mode levels (a; 0, ν_2, 0) and (s; 0, ν_2, 0), respectively, with ν_2 = 0,...,13. The nearly horizontal lines correspond to the progressions (a; ν_1, 0, 0) and (s; ν_1, 0, 0) with ν_1 = 0, 1,.... The lines with negative slopes correspond to (a; 0, 0, ν_3) and (s; 0, 0, ν_3) progression with ν_3 = 0,...,3.

The lower panel of Fig. 1 shows the B_ν rotational constants. The two families of the levels localized in the symmetric and asymmetric wells are also clearly distinguishable. However, the ν-progressions are less obvious to identify compared to the graph of the A_ν rotational constants. The third constant, C_ν, is not shown as it behaves similarly to B_ν. Both of them generally decrease with energy as the corresponding moments of inertia increase due to excited vibrations.

Near the dissociation limit, about −150 to 0 cm^{-1} with respect to the ^{16}O + $^{16}O^{18}O$ dissociation limit, wave functions of certain levels delocalized between the potential wells, have non-negligible amplitudes at liner geometries of the three

Table 3 Energies (in cm^{-1}) of highly excited vibrational levels of the A irrep of $^{50}O_3$ computed with respect to the ZPE of $^{16}O^{18}O^{16}O$. The table also gives averaged values of $\langle\phi\rangle$ (in degrees) and $\langle r_{66}\rangle$ (in Bohr). i is the ranking number with increasing energy. ZPE($^{50}O_3$) = 1406.87 cm^{-1}, corresponding to the 686 arrangement in well-III. The lowest (000) level of the 668/866 arrangement in well-I and well-II is at 1421.09 cm^{-1} above the bottom of the wells

i	E	$\langle\phi\rangle$	$\langle r_{66}\rangle$	Well	i	E	$\langle\phi\rangle$	$\langle r_{66}\rangle$	Well	i	E	$\langle\phi\rangle$	$\langle r_{66}\rangle$	Well
346	8020.52	−36.23	2.49	C_s	384	8288.59	80.09	4.49	C_{2v}	422	8425.38	50.24	6.16	C_{2v}
347	8021.03	84.30	4.26	C_{2v}	385	8289.76	−32.18	2.68	C_s	423	8427.76	−7.68	4.39	Mix
348	8038.22	−35.31	2.49	C_s	386	8295.88	−30.48	3.01	C_s	424	8436.74	−27.31	3.56	C_s
349	8042.32	79.52	4.43	C_{2v}	387	8295.96	66.22	5.23	C_{2v}	425	8439.56	−27.41	2.94	C_s
350	8045.75	−28.57	2.67	C_s	388	8305.83	−28.78	2.68	C_s	426	8441.02	−31.79	2.98	C_s
351	8045.88	−32.75	2.47	C_s	389	8312.91	78.23	4.54	C_{2v}	427	8443.02	−70.50	2.30	C_s
352	8051.53	−29.92	2.63	C_s	390	8313.49	−50.67	2.40	C_s	428	8443.32	50.11	6.50	C_{2v}
353	8067.98	79.46	4.38	C_{2v}	391	8329.37	−10.27	4.04	C_s	429	8447.00	−41.13	3.12	C_s
354	8076.77	−30.60	2.61	C_s	392	8331.20	−33.15	2.54	C_s	430	8447.90	−19.40	4.44	C_s
355	8080.92	−29.16	2.63	C_s	393	8331.71	−44.14	2.45	C_s	431	8450.94	43.48	6.27	Mix
356	8085.28	−28.35	2.68	C_s	394	8332.43	68.23	5.28	C_{2v}	432	8451.28	−39.42	3.06	C_s
357	8088.58	−32.05	2.52	C_s	395	8344.94	76.02	4.72	C_{2v}	433	8454.07	33.06	6.46	Mix
358	8090.07	80.68	4.37	C_{2v}	396	8347.24	−31.82	2.64	C_s	434	8459.02	−8.08	4.59	Mix
359	8104.67	−35.20	2.48	C_s	397	8353.86	−33.24	2.59	C_s	435	8461.93	19.05	5.52	Mix
360	8131.44	−35.56	2.48	C_s	398	8354.99	73.89	4.99	C_{2v}	436	8464.91	−13.85	3.99	C_s
361	8132.83	77.43	4.44	C_{2v}	399	8356.34	−32.46	3.02	C_s	437	8466.93	17.34	5.47	Mix
362	8139.12	−28.64	2.70	C_s	400	8360.27	81.88	4.40	C_{2v}	438	8467.93	−17.46	4.25	C_s
363	8140.23	87.23	4.27	C_{2v}	401	8360.92	−19.93	3.77	C_s	439	8471.53	−14.33	4.29	C_s
364	8146.69	82.30	4.38	C_{2v}	402	8366.36	−19.04	3.25	C_s	440	8473.06	−28.12	3.32	C_s
365	8155.08	−32.04	2.54	C_s	403	8366.56	39.84	4.79	Mix	441	8474.69	38.27	5.83	Mix
366	8158.20	−30.98	2.61	C_s	404	8372.43	71.57	4.83	C_{2v}	442	8477.68	-14.16	4.20	C_s
367	8173.61	−31.87	2.59	C_s	405	8375.20	75.73	4.46	C_{2v}	443	8478.56	16.93	6.12	Mix
368	8182.34	81.15	4.32	C_{2v}	406	8377.33	13.55	4.75	Mix	444	8481.43	32.21	6.66	Mix
369	8191.68	−33.99	2.47	C_s	407	8383.44	44.38	5.69	Mix	445	8482.38	−32.26	3.42	C_s
370	8192.52	−38.58	2.44	C_s	408	8384.32	−39.61	2.48	C_s	446	8484.64	−59.37	2.56	C_s
371	8195.96	82.50	4.36	C_{2v}	409	8387.78	3.16	5.07	Mix	447	8486.61	67.60	5.89	C_{2v}
372	8200.10	81.61	4.39	C_{2v}	410	8389.49	−54.69	2.48	C_s	448	8489.27	−22.71	3.95	C_s
373	8203.49	−31.39	2.62	C_s	411	8391.93	63.18	6.45	C_{2v}	449	8489.80	−11.22	4.72	C_s
374	8219.98	−31.78	2.59	C_s	412	8400.28	−42.37	2.81	C_s	450	8490.79	31.64	6.87	Mix
375	8238.45	−27.01	2.75	C_s	413	8403.38	−51.78	2.51	C_s	451	8491.54	−32.61	3.14	C_s
376	8241.48	80.50	4.33	C_{2v}	414	8406.16	−15.08	4.03	C_s	452	8492.59	−37.70	2.73	C_s
377	8242.45	−32.39	2.61	C_s	415	8410.62	−50.30	2.45	C_s	453	8493.49	30.64	6.38	Mix
378	8257.65	−28.54	2.79	C_s	416	8411.14	66.38	5.82	C_{2v}	454	8496.70	−24.69	4.02	C_s
379	8268.48	74.70	4.69	C_{2v}	417	8418.82	−38.24	2.73	C_s	455	8497.35	53.62	5.33	C_{2v}
380	8274.06	−32.58	2.55	C_s	418	8419.97	27.81	5.93	Mix	456	8500.15	34.01	6.59	Mix
381	8274.75	77.70	4.59	C_{2v}	419	8423.07	−11.51	4.23	C_s	457	8501.67	22.76	5.88	Mix
382	8283.80	−36.06	2.51	C_s	420	8423.74	64.57	5.90	C_{2v}	458	8502.16	−23.92	3.92	C_s
383	8288.17	−16.37	3.60	C_s	421	8424.96	−27.30	2.93	C_s	459				

atoms. At such geometries, one of the moments of inertia about the axis of symmetry becomes zero. As the result, for these levels, the expectation value A_ν looses the meaning of a rotational constant and cannot be used in calculations of rotational energies of a rigid rotor.

3.4 Delocalized states and tunneling between the wells

At energies above approximately 8350 cm^{-1} there appear series of states that are delocalized over the potential wells. Fig. 2 shows several characteristic expectation values of excited vibrational levels averaged over vibrational wave functions (4) and (5) depending on the level energy. The upper panel shows A_ν, the largest of the three rotational constants (A_ν, B_ν, and C_ν), while the smallest rotational constant, $\langle C_\nu\rangle$, is shown on the second panel from the top. The third panel from the top shows the average value of the hyperangle ϕ. Changing the hyperangle ϕ in the interval $[0;2\pi]$ corresponds to the ozone nuclear geometrical configuration moving continuously between the three potential wells.[31–33,35,36] In the calculation of the averaged value $\langle\phi\rangle = \langle\nu|\phi|\nu\rangle$, only one half of the full interval of 2π was used as this is sufficient to distinguish between levels localized in the symmetric $^{16}O^{18}O^{16}O$ well (C_{2v} point group isotopomer in the traditional approach) and those in the asymmetric $^{16}O^{16}O^{18}O/^{18}O^{16}O^{16}O$ wells (C_s point group isotopomer in the traditional approach). As one can see, the $\langle\phi\rangle$ value for all levels below 8250 cm^{-1} is either negative (near −30 degrees) or positive (near 80 degrees), which correspond to the geometries of minima of the $^{16}O^{16}O^{18}O/^{18}O^{16}O^{16}O$ wells and the $^{16}O^{18}O^{16}O$ well. The lowest panel of Fig. 2 gives the variation of $\langle r_{66}\rangle$ – the averaged distance between the two ^{16}O nuclei in the $^{50}O_3$ isotopologue. The two lowest panels clearly distinguish the levels localized in C_{2v} or C_s wells and the delocalized levels.

Below 8250 cm^{-1}, $\langle r_{66}\rangle$ is either about 4.5 or 2.5 Bohr corresponding to the symmetric and asymmetric wells. Above 8250 cm^{-1}, the tunneling effect mixes wave functions situated in different wells for certain levels. Also, in general, distances between the atoms become larger when energies of the levels approach the lowest dissociation limit of $^{16}O^{18}O$ + ^{16}O near 8505 cm^{-1}.

Tables 3 and 4 give numerical values for the energies, $\langle\phi\rangle$, and $\langle r_{66}\rangle$ values for highly-excited bound levels. A full set of levels is given in ESI.†

Table 4 Same as in Table 3 for *B* levels

i	*E*	⟨ϕ⟩	⟨r_{66}⟩	Well	*i*	*E*	⟨ϕ⟩	⟨r_{66}⟩	Well	*i*	*E*	⟨ϕ⟩	⟨r_{66}⟩	Well
317	8038.20	−35.32	2.49	C_s	354	8295.88	−31.58	2.99	C_s	391	8440.90	−19.26	3.38	C_s
318	8045.74	−28.57	2.67	C_s	355	8305.83	−28.78	2.68	C_s	392	8441.72	33.78	5.46	Mix
319	8045.88	−32.75	2.47	C_s	356	8307.16	70.11	5.05	C_{2v}	393	8446.85	−3.75	4.28	Mix
320	8051.53	−29.92	2.63	C_s	357	8313.51	−50.67	2.40	C_s	394	8447.33	−14.72	3.64	C_s
321	8057.18	80.91	4.33	C_{2v}	358	8329.33	−10.30	4.04	C_s	395	8448.52	24.33	4.56	Mix
322	8063.74	80.53	4.40	C_{2v}	359	8331.20	−33.22	2.54	C_s	396	8450.39	44.09	6.36	Mix
323	8076.78	−30.59	2.61	C_s	360	8331.70	−44.02	2.46	C_s	397	8450.80	−31.74	3.24	C_s
324	8080.92	−29.16	2.63	C_s	361	8331.89	69.23	5.11	C_{2v}	398	8454.08	33.77	6.40	Mix
325	8081.93	80.97	4.35	C_{2v}	362	8342.69	74.87	4.83	C_{2v}	399	8458.98	−9.51	4.52	Mix
326	8085.27	−28.35	2.68	C_s	363	8347.25	−31.81	2.64	C_s	400	8462.07	10.29	5.03	Mix
327	8088.58	−32.05	2.52	C_s	364	8353.86	−33.25	2.59	C_s	401	8464.54	−0.97	4.26	Mix
328	8104.67	−35.20	2.48	C_s	365	8354.67	72.58	5.08	C_{2v}	402	8466.44	30.47	5.38	Mix
329	8131.43	−35.56	2.48	C_s	366	8356.36	−32.15	3.03	C_s	403	8468.11	−15.84	4.22	C_s
330	8134.76	79.49	4.42	C_{2v}	367	8360.92	−19.98	3.76	C_s	404	8468.99	75.39	4.51	C_{2v}
331	8139.10	−28.64	2.70	C_s	368	8366.43	−36.61	2.71	C_s	405	8470.40	51.52	5.30	C_{2v}
332	8142.12	78.54	4.42	C_{2v}	369	8366.60	69.23	4.46	C_{2v}	406	8472.52	−8.82	4.26	Mix
333	8155.08	−32.04	2.54	C_s	370	8367.62	64.98	5.50	C_{2v}	407	8473.92	−42.22	2.90	C_s
334	8158.19	−30.98	2.61	C_s	371	8376.57	12.48	4.89	Mix	408	8476.84	−49.31	2.73	C_s
335	8162.04	80.55	4.33	C_{2v}	372	8381.11	41.56	5.42	Mix	409	8477.81	44.40	6.42	Mix
336	8173.60	−31.88	2.59	C_s	373	8384.37	−39.55	2.46	C_s	410	8478.06	−21.45	4.16	C_s
337	8191.68	−34.00	2.47	C_s	374	8387.39	7.82	5.17	Mix	411	8479.16	17.80	5.64	Mix
338	8192.49	−38.58	2.44	C_s	375	8389.12	53.80	6.43	C_{2v}	412	8481.90	36.56	6.85	Mix
339	8195.48	83.30	4.26	C_{2v}	376	8390.39	−53.12	2.45	C_s	413	8482.73	−26.72	3.53	C_s
340	8203.48	−31.39	2.62	C_s	377	8401.18	−30.98	3.01	C_s	414	8488.41	−44.91	2.79	C_s
341	8206.66	79.42	4.38	C_{2v}	378	8403.84	67.92	5.65	C_{2v}	415	8490.07	13.95	6.13	Mix
342	8219.97	−31.77	2.59	C_s	379	8406.00	−21.27	3.65	C_s	416	8490.75	33.46	6.94	Mix
343	8237.78	76.39	4.58	C_{2v}	380	8407.41	−50.60	2.75	C_s	417	8491.82	−29.69	2.92	C_s
344	8238.43	−26.98	2.75	C_s	381	8411.29	−55.61	2.37	C_s	418	8493.51	−20.51	4.05	C_s
345	8242.44	−32.41	2.61	C_s	382	8418.86	−37.85	2.74	C_s	419	8493.95	10.28	5.71	Mix
346	8257.62	−28.56	2.78	C_s	383	8419.89	48.96	6.06	Mix	420	8497.11	34.86	6.04	Mix
347	8266.77	78.27	4.37	C_{2v}	384	8419.99	44.17	5.93	Mix	421	8497.81	−5.42	4.25	Mix
348	8274.07	−32.58	2.55	C_s	385	8423.09	−11.59	4.22	C_s	422	8500.43	−26.51	4.26	C_s
349	8274.79	84.24	4.31	C_{2v}	386	8424.82	47.45	6.39	Mix	423	8500.94	−19.14	4.73	C_s
350	8283.78	−36.07	2.51	C_s	387	8424.99	−26.96	2.94	C_s	424	8502.46	11.69	5.53	Mix
351	8284.78	63.49	5.46	C_{2v}	388	8427.79	−7.94	4.39	Mix	425				
352	8288.18	−16.45	3.60	C_s	389	8436.74	−26.69	3.58	C_s	426				

By examining the dependence of vibrational wave functions on the hyper-radius ρ and two hyperangles θ, ϕ we distinguish several cases of delocalization with characteristic examples given in Fig. 3–7.

Note that for the sake of simplicity of the graphical representation in these figures, the directions of variations of the coordinates are guided here by the Cartesian set of arrows. The green ϕ-arrow points the direction linking the three potential wells: the central well corresponds to the well-III (C_{2v} geometrical configuration) and two edge wells correspond to well-I and well-II (C_s geometrical configuration). The red ρ-arrow points the direction of a delocalization out of the wells. The

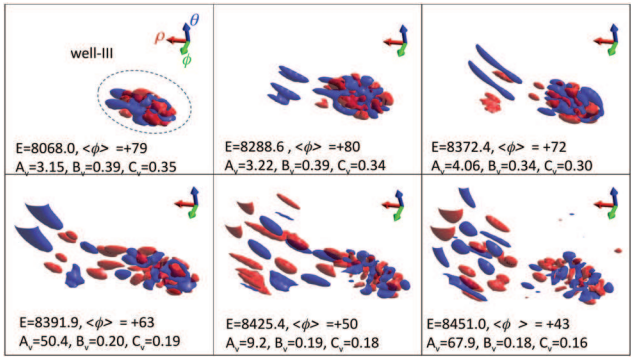

Fig. 3 Series of *A*-type vibrational wave functions (4) progressively delocalized from symmetric 686 well-III with positive hyperangle ϕ values. Nodal structures towards the left-hand tails correspond to increasing ψ amplitudes at flat range of the PES for large hyper-radius ρ. Vibrational energies, *E*, and state-specific rotational constants *A*, *B*, *C* are given in cm^{-1}, the angle ⟨ϕ⟩ is in degrees in this figure and in Fig. 4–7.

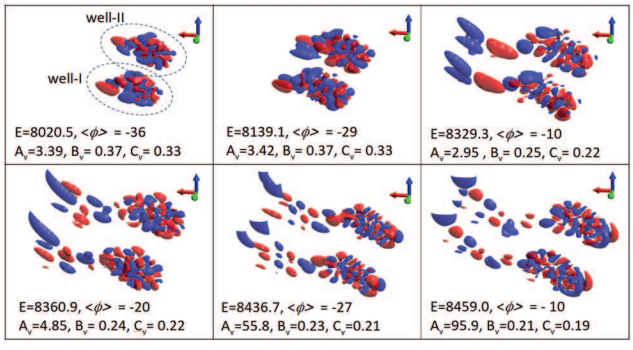

Fig. 4 Series of *A*-type vibrational wave functions (5) progressively delocalized from asymmetric 668/866 well-I and well-II with negative values of the hyperangle ϕ. Nodal structures towards the left-hand tails correspond to increasing ψ amplitudes at flat range of the PES for large hyper-radius ρ.

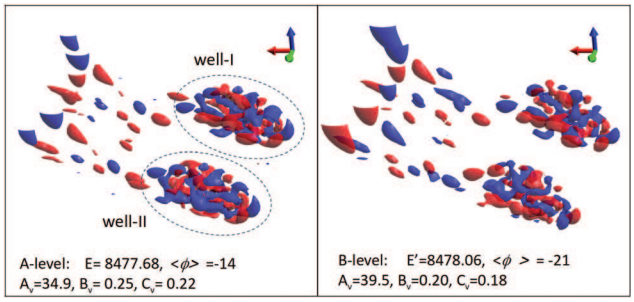

Fig. 5 Example of lifted A/B degeneracy for vibrational levels of $^{50}O_3$ ozone isotopomers due to the interaction between asymmetric C_s configurations of the potential well-I and well-II resulting to the splitting of $\Delta E = E' - E = 0.325$ cm^{-1} in rovibrational sub-band centers.

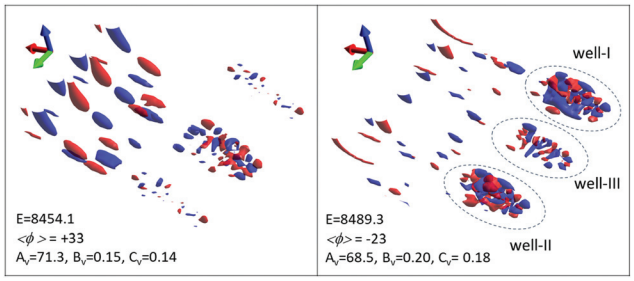

Fig. 6 Delocalized A-type vibrational wave functions (6) of $^{50}O_3$ with significant amplitudes in all three potential wells. Left-hand panel corresponds to the dominant contributions in the symmetric well-III (686), the right-hand panel to the dominant contribution in the asymmetric well-I and well-II (668/866). Nodal structures towards the left-hand tails correspond to increasing ψ amplitudes in the flat range of the PES for large hyper-radius ρ.

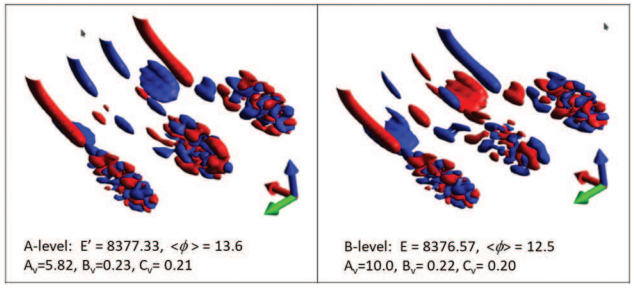

Fig. 7 Example of lifted A/B degeneracy for vibrational levels of $^{50}O_3$ ozone isotopomers due to the interaction between all three potential well-I, well-II, and well-III resulting to the splitting of $\Delta E = E' - E = 0.76$ cm^{-1} in rovibrational sub-band centers.

blue θ-arrow corresponds to the bending progression, for which ρ simultaneously increases.

The wave functions are shown in the hyperspherical coordinates as surfaces of equal magnitude with the red and blue colors corresponding to positive and negative values of $\psi_v(\rho,\theta,\phi)$. The wave functions are normalized to unity in the hyperspherical space. The interval of variation of ρ for the chosen magnitude of ψ is approximately from 3.5 to 7 Bohr. The hyperangle ϕ changes in the interval from $-\pi/2$ to $3\pi/2$ with the symmetric-well minimum situated in the middle of the interval at $\phi = \pi/2$ (and in the middle of the figures). Minima of the asymmetric wells $^{16}O^{16}O^{18}O$ and $^{18}O^{16}O^{16}O$ are located at $\phi = -\pi/6$ and $\phi = 7\pi/6$. In the figures, these two minima are situated on the two sides from the minimum of the symmetric well, so that the shown wave functions look symmetric.

Fig. 3 and 4 show examples of series of progressively delocalized states where the wave functions come out of the wells towards the flat range of the potential surface near the dissociation threshold, but without mixing of C_{2v} and C_s channels. In these cases the average $\langle\phi\rangle$ values stay either positive (C_{2v} configuration), or negative (C_s configuration) in Fig. 2.

Another case shown in Fig. 5 corresponds to the interaction between two asymmetric C_s configurations $^{16}O^{16}O^{18}O$ and $^{18}O^{16}O^{16}O$ situated in well-I and well-II. Let us remind that the barriers between these wells near the equilibrium geometries are very high but these barriers rapidly decrease in the direction towards the dissociation channels. Consequently, both A-type and B-type wave functions (5) for highly excited states can have significant amplitude at the flat potential range along the curvilinear path between well-I and well-II. The corresponding interaction between well-I and well-II results in an A/B splitting which amounts to about 0.3 to 0.6 cm^{-1} for some states around 8400 cm^{-1}.

The third case of delocalization corresponds to the mixing of quantum states among all three wells. In this case the vibrational wave functions take the form

$$\begin{aligned}|\mathrm{m};\nu,A\rangle &= d_s^A|\mathrm{s};\nu',A\rangle + d_a^A|\mathrm{a};\nu'',A\rangle \\ &= d_s^A|\nu',A\rangle_{III} + \frac{d_a^A}{\sqrt{2}}(|\nu''\rangle_I + |\nu''\rangle_{II})\end{aligned} \quad (6)$$

$$\begin{aligned}|\mathrm{m};\nu,B\rangle &= d_s^B|\mathrm{s};\nu',B\rangle + d_a^B|\mathrm{a};\nu'',B\rangle \\ &= d_s^B|\nu',B\rangle_{III} + \frac{d_a^B}{\sqrt{2}}(|\nu''\rangle_I - |\nu''\rangle_{II})\end{aligned} \quad (7)$$

The left-hand symbol "m" in the wave functions stands for "mixed", whereas "s" means localized in the symmetric well-III, and "a" means localized in the asymmetric wells I or II. Note that neither normal ν, ν', ν'' nor local mode assignments are good quantum numbers at these energies, contrary to the symmetry types A or B that remain exact. The wave functions (4) and (5) relative to 686 or 668 rearrangements play here the role of the basis set of the full $^{50}O_3$ three-wells wave functions. Near the dissociation limits, wave functions of certain levels become completely delocalized between the three wells. Above 8350 cm^{-1}, the value of $\langle\phi\rangle$ for certain levels is quite different from -30 or 85 degrees, which means that these levels are already delocalized between the symmetric and asymmetric wells as is clearly seen in Fig. 2.

The mixing coefficients d_s^Γ and d_a^Γ in eqn (6) and (7) determine which configuration dominates. Two examples with

dominant contribution of either symmetric or asymmetric potential wells are given in Fig. 6. For some cases the contributions between 686 and 668/866 wells are nearly equally shared (Fig. 7). This figure shows an example of *A*/*B* splitting of vibrational levels in the case where vibrational parts of total rovibrational wave functions (2) is completely shared among well-I, well-II and well-III. This will have an impact on rovibrational patterns of observable bands as discussed above.

The wave functions of Fig. 5–7 have significant probability densities at large values of ρ without restricting the motion along the ϕ and θ-hyperangles: for large ρ, the motion for the corresponding states along the hyperangles is not localized in the flat range of the potential energy near the dissociation threshold. The situation corresponds to the motion of an oxygen atom separated from the O_2 molecule by a relatively large distance, such that the atom can move almost freely around the diatomic partner, "roaming"[64,65] around it.

3.5 Possible consequences for analyses and modelling of experimental spectra

According to Table 2, the $J = 0$ levels of *B*-symmetry type are not spin-allowed in case of the ozone isotopologues made of ^{16}O and ^{18}O atoms. This is the well-known repercussion of spin weights associated to boson nuclei. However, rotational patterns of these vibrational levels and rovibrational sub-bands do exist, as it was discussed in Section 3.2. The calculated "missing" vibrational $E^B_{\nu,J=0}$ levels are useful for practical applications as they determine the corresponding sub-bands centers, which can be deduced from analyses of experimental spectra.[4,8,11,59–61]

The splitting between calculated $E^A_{\nu,J=0}$ and $E^B_{\nu,J=0}$ high-energy levels due to the delocalization of wave functions considered in Section 3.4 will thus result in new types of perturbations in observable spectra. The first consequence is that centers of parallel and perpendicular sub-bands in hybrid bands of asymmetric 668 isotopomer[59–61] will be shifted one with respect to another. The second consequence is that rotational constants of these sub-bands will change in a different way. These findings suggests that more complicated effective spectroscopic Hamiltonian models with respect to the existing ones[4,8,11,59–61] will be required in order to assign *J*-progressions.

Finally, the most drastic impact for future analyses of experimental spectra above 8000 cm^{-1} is due to the fact that $^{16}O^{16}O^{18}O$ and $^{16}O^{18}O^{16}O$ isotopomers could no more be treated separately. Thus, new effective spectroscopic models accounting for the interaction of the corresponding isotopic bands have to be developed in order to assign experimental spectra near the dissociation threshold.

4 The main $^{48}O_3$ isotopologue

4.1 Symmetry considerations, rovibrational bands and sub-bands

For the symmetric isotopologue of ozone $^{48}O_3$, composed of three identical nuclei ^{16}O, the full symmetry is described by the three-particle permutation-inversion group $S_3 \times I$, while purely vibrational levels are described by the S_3 group. For high energies all permutations are feasible, which makes this group equivalent to $D_{3h}(M)$, where *M* stands for molecular symmetry group.[62] This group has six irreducible representations - four one-dimensional irreps A_1', A_2', A_1'', A_2'' and two two-dimensional irreps E', E''. The vibrational functions have positive parity in the group, *i.e.* they belong to either A_1', A_2' or E' irreps (A_1, A_2 or E irreps in the S_3 subgroup), while both prime and double-prime irreps exist for rotationally excited states. We shall use the definitions for the symmetry types of the previous work[36] where the reader can find more detailed discussions.

Table 5 Symmetry of $^{48}O_3$ rotational states in $S_3 \times I$

K	Γ
0	A_1' (J even), A_2' (J odd)
1, 5, 7, 11...	E''
2, 4, 8, 10...	E'
3, 9...	$A_1'' \oplus A_2''$
6, 12...	$A_1' \oplus A_2'$

In $S_3 \times I$ rotational states are classified according to J and K, where K refers to the projection of J on the axis perpendicular to the molecular plane. Rotational states transform pairwise since $K = |\pm k|$, except for $K = 0$. States are degenerate, E, unless K is a multiple of 3, in which case they transform as $A_1 \oplus A_2$. The parity of rotational states, to be added to these labels, is $p = (-1)^K$. Therefore we obtain the following classification, Table 5.

The ground electronic state is of the A_1' irrep in this group, the spin-allowed irreps for vibration–rotation functions are A_1' and A_1''. Equilibrium geometrical configurations in each of three individual potential wells have three different principal moments of inertia $I_a < I_b < I_c$, where the *c*-axis is orthogonal to the molecular plane. Consequently, the rotational states have to be characterized by the asymmetric-rotor quantum numbers J, K_a, K_c and the rovibrational wave functions can be written in the form (2) as in the case of the $^{48}O_3$ isotopologue. Indistinguishability of the three boson atoms and the requirement of the total symmetry types A_1' and A_1'' imposes restrictions on allowed combinations of rotational and vibrational wave functions.

To connect these results with the asymmetric top rotational functions $J_{K_aK_c}$ of ozone, we note that the *a* and *b*-axes are in the molecular plane, while the *c*-axis is perpendicular. The symmetry is thus determined by J and K_c. A summary of the allowed combinations of vibrational and rotational states is given in Table 6. Care must be taken when combining the degenerate vibrational states with degenerate rotational states. The direct product $E \otimes E = A_1 \oplus A_2 \oplus E$, but only the combination that yields A_1 symmetry is allowed. This eliminates one of the asymmetric top states. For ν_3 even, only the rotational functions J_{ee} and J_{oo} yield a rovibrational function of symmetry A_1. For ν_3 odd, the allowed rotational functions are J_{eo} and J_{oe}.

It follows from Table 6 that only A_1' symmetry types are spin-allowed for $J = 0$ states. However, a computation of missing

Table 6 Allowed combinations of irreps for rotational and vibrational wave functions of $(^{16}O)_3$ and $(^{18}O)_3$. The last columns give examples of allowed rotational states for $J \leq 3$. The underlined states are allowed for ν_3 even (spin statistical weight 1) and forbidden for ν_3 odd. The non-underlined states are allowed for ν_3 odd (spin statistical weight 1) but forbidden for ν_3 even. See text for explication

					Rotational states examples			
Γ_{rovib}	Γ_{vib}	Γ_{rot}	Rotational states		$J = 0$	$J = 1$	$J = 2$	$J = 3$
A_1'	A_1	A_1'	$\underline{J_{eK_c}}$	$K_c = 0, 6, \ldots$	$\underline{0_{00}}$		$\underline{2_{20}}$	
A_1''		A_1''	$\underline{J_{oK_c}}$	$K_c = 3, 9, \ldots$				$\underline{3_{13}}$
A_1'	A_2	A_2'	J_{oK_c}	$K_c = 0, 6, \ldots$		1_{10}		3_{30}
A_1''		A_1''	J_{eK_c}	$K_c = 3, 9, \ldots$				3_{03}
A_1'	E	E'	$\underline{J_{eK_c}} \oplus \underline{J_{oK_c}}$	$K_c = 2, 4, 8, \ldots$			$\underline{2_{01}} \oplus 2_{12}$	$\underline{3_{22}} \oplus 3_{12}$
A_1''		E''	$\underline{J_{eK_c}} \oplus \underline{J_{oK_c}}$	$K_c = 1, 5, 7, \ldots$		$1_{01} \oplus \underline{1_{11}}$	$2_{21} \oplus \underline{2_{11}}$	$3_{21} \oplus \underline{3_{31}}$

"vibrational levels" of A_2' and E' irreps is useful for analyses of rovibrational bands because rotational patterns of these vibrational level do exist. Each of A_1, A_2 and E vibrational levels determines the center of the corresponding observable vibration–rotation sub-band. In this sense, a consideration of the quasi-degeneracy between these levels at the bottom of the potential wells and of their splitting at high energies due to interactions among three potential wells is meaningful because it permits understanding of related perturbations in observable bands.

Similarly to the case of the asymmetric isotopologue (discussed in Sections 3.3 and 3.4), there is a quasi-degeneracy for some of the levels, situated deep in the potential wells. Let us first consider eigen-values of purely vibrational Hamiltonian, neglecting the spin effects for the moment. In case of $^{48}O_3$, the three potential wells are equivalent, and in the absence of an appreciable tunneling there would be a triple degeneracy of the levels situated in different wells. From the wave functions of the three degenerate vibrational levels, one can construct wave functions with correct symmetry properties with respect to indistinguishability of the three nuclei: a pair of wave functions of the E irrep and another wave function of a A_1 or A_2 irrep, depending on the symmetry of the initial wave function. Namely, using the approximate quantum numbers (ν_1, ν_2, ν_3) for wave functions in each well, the levels with even ν_3 will produce an E pair and a level of the A_1 irrep; the levels with odd ν_3 will also produce an E pair and a level of the A_2 irrep. For convenience, we will use the notations $|\nu_1\nu_2\nu_3 A_1\rangle$, $|\nu_1\nu_2\nu_3 A_2\rangle$, and $|\nu_1\nu_2\nu_3 E\rangle$ for the levels deep in the potential wells but having correct transformation properties under permutation of identical nuclei. For the sake of simplicity, the primes for all vibrational irreps are omitted here, because all vibrations are invariant under the inversion operation.

It is instructive to consider a correlation with symmetry notations which are traditionally employed in ozone spectroscopy in a one-potential-well approximation.[4,8] In the one-well approximation, the ozone molecule belongs to the C_{2v} point group with vibrations transforming according to A_1 (for even ν_3) and B_1 (for odd ν_3) irreps of C_{2v}. As for $^{50}O_3$ in Section 3.3, let us consider "cold" bands (3) corresponding to the transitions from the ground vibrational state $\nu' = 0$, which are the strongest ones in atmospheric conditions. In the C_{2v} point group, the transition to rotational levels of B_1 vibrations give rise to "parallel" bands whereas transitions to rotational levels of A_1 vibrations give rise to "perpendicular" bands.

In the full symmetry approach accounting for the three wells, we have to replace for vibrational levels

$$A_1(\text{group } C_{2v}) \rightarrow A_1, E(\text{sub-group } S_3), \quad (8)$$

$$B_1(\text{group } C_{2v}) \rightarrow A_2, E(\text{sub-group } S_3), \quad (9)$$

where the left-hand notation stands for the one-well approach.

This means that a cold perpendicular band (with $\Delta\nu_3$ even) corresponding to A_1 upper vibrational levels in the one-well approximation has to be considered as composed of two sub-bands corresponding to A_1 and E vibrational levels in the S_3 group. A cold parallel band (with $\Delta\nu_3$ odd) corresponding to B_1

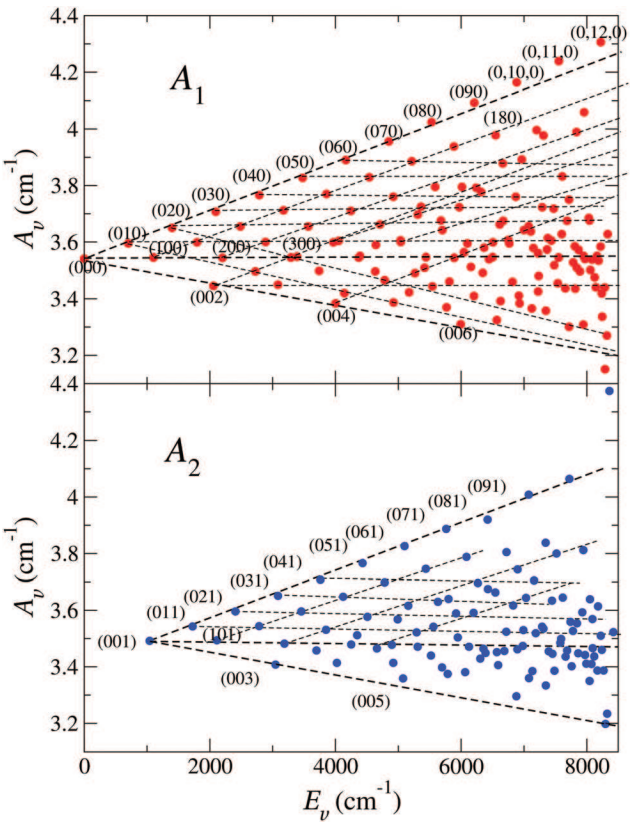

Fig. 8 Rotational constants $\langle A_\nu \rangle$ of the $^{48}O_3$ bound states. The levels of the A_1 and A_2 irreps of $S_3 \times I$ group are shown in separate panels.

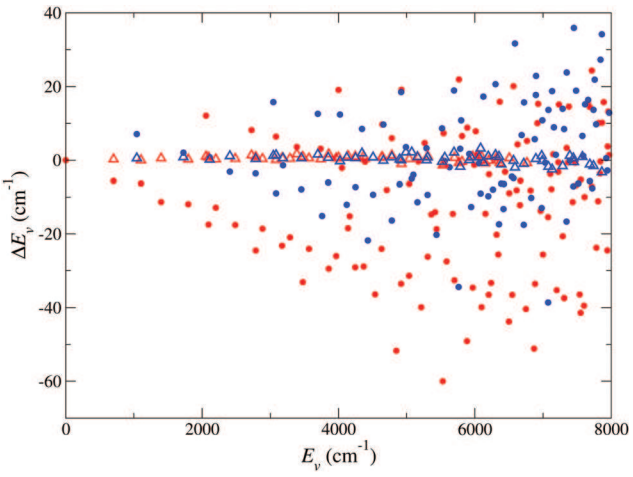

Fig. 9 Observed – calculated deviations of the energies of $^{46}O_3$ obtained in this study with the experimental data[4–6,9–11,13,49,66] (open red and blue triangles) and comparison with the calculation residuals of ref. 67 (closed red and blue circles). The horizontal axis in the plot gives the level energies, the vertical axis is the difference between the energies in the two studies. Red symbols correspond to the A_1 levels, blue symbols represent the A_2 levels. The difference between the results is attributed to the different PESs used in the studies.

upper vibrational levels in the one-well approximation has to be considered as composed of two sub-bands corresponding to A_2 and E vibrational levels in S_3.

There is no degeneracy or quasi-degeneracy between the A_1 and B_1 vibrational levels of the C_{2v} point group. In a full symmetry approach, the couples of vibrational sub-levels A_1/E and A_2/E are near-degenerate deep in the potential wells. Consequently, the corresponding sub-band centers coincide. However, at high vibrational energies there occurs splitting of these sub-levels and of the observable rovibrational sub-band centers.

Similarly to the asymmetric isotopologue, energies, wave functions, and expectation values of several quantities were computed using the approach briefly discussed above. Fig. 8 shows energies and largest rotational constants $\langle A_\nu \rangle$ for the A_1 and A_2 levels. Energies and rotational constants for the E levels at energies below 8200 cm^{-1} are almost the same as for the third levels of the triad, A_1 or A_2.

Fig. 9 compares the energies obtained in this study with experiment.[4–6,9–11,13,49,66] The agreement with the experimental data is within 1 cm^{-1}. The figure also shows a comparison with calculations of Teplukhin and Babikov,[67] where a different PES, by Dawes *et al.*[44] was used, and the same numerical approach combining the hyperspherical coordinates and adiabatic separation of the hyper-radius and hyperangles. The significant disagreement in energies obtained in this study and in ref. 67 is most likely due to the differences in the employed PESs.

4.2 Delocalized states, tunneling between the wells and splitting of A/E sub-bands

As levels approach the dissociation limit, the vibrational dynamics may have a large amplitude along internuclear distances between the nuclei or/and may involve linear geometries, where the potential barrier between different equivalent configurations is small such that a transition between different wells becomes possible, similar to the case of the asymmetric isotopologue. For such excited levels, tunneling lifts the quasi-degeneracy between the E and A_1 or A_2 levels. However, the E state stays doubly degenerate due to the S_3 symmetry of the system.

The degeneracy as well as the splitting between the E, A_1, and A_2 levels can be seen in Tables 7–9.

For example, the A_1 level with energy 8031.57 cm^{-1} (Table 7) is degenerate with a level of the E irrep (the first line in Table 9), whereas the A_1 level with E_ν = 8369.02 cm^{-1} has a quite different energy compared to its E "partner" with E_ν = 8370.70 cm^{-1}. Similar examples are found for the A_1/E splitting, such as between E_ν = 8360.18 cm^{-1} and E_ν = 8360.74 cm^{-1}. Fig. 11 gives an overview picture of the splittings, showing expectation values of the rotational constants $\langle A_\nu \rangle$ and the hyper-radius ρ for the levels near the dissociation limit. One can see that the splitting is rather small below 8350 cm^{-1} and becomes appreciable for energies above. At this energy, the tunneling probability becomes non-negligible.

Table 7 Energies E_ν (in cm^{-1}), the largest rotational constants $\langle A_\nu \rangle$ (in cm^{-1}), and averaged values of the hyper-radius (in Bohr) of highly-excited vibrational levels of the A_1 irrep, with respect to the ZPE for the main ozone isotopologue $^{48}O_3$. ZPE($^{48}O_3$) = 1453.29 cm^{-1}, which agrees within all six decimal places with the value in one-well calculations by Tyuterev *et al.*,[5] where it was quoted as 1443.52 cm^{-1} with respect to the reference E_0 geometrical grid point (r_1 = r_2 = 2.4 Bohrs, θ = 117°), which is above the minimum of the TKTHS PES by 9.77 cm^{-1}

i	E	$\langle A_\nu \rangle$	$\langle \rho \rangle$	i	E	$\langle A_\nu \rangle$	$\langle \rho \rangle$	i	E	$\langle A_\nu \rangle$	$\langle \rho \rangle$	i	E	$\langle A_\nu \rangle$	$\langle \rho \rangle$
118	7957.31	4.1	4.2	130	8238.75	3.4	4.3	142	8406.97	101.9	6.4	154	8473.41	90.8	7.0
119	7970.66	3.5	4.3	131	8244.93	3.3	4.6	143	8408.51	15.4	6.7	155	8477.69	31.1	5.8
120	8031.57	3.7	4.3	132	8273.85	3.1	5.2	144	8414.27	16.2	6.4	156	8480.15	10.2	7.7
121	8043.32	3.7	4.3	133	8285.43	3.4	4.3	145	8431.04	40.0	6.3	157	8484.09	50.2	6.4
122	8056.37	3.5	4.3	134	8289.78	3.1	5.1	146	8434.17	18.7	5.3	158	8489.00	71.7	7.8
123	8081.19	3.5	4.3	135	8318.92	3.3	5.0	147	8438.84	80.5	6.4	159	8490.36	42.3	9.1
124	8124.72	3.5	4.4	136	8332.01	3.6	5.4	148	8443.14	5.9	4.4	160	8494.12	49.5	5.5
125	8144.46	3.4	4.4	137	8353.94	5.8	5.1	149	8449.77	59.2	6.5	161	8496.77	26.3	11.2
126	8161.89	3.5	4.3	138	8355.59	6.6	5.4	150	8453.41	28.2	5.9	162	8497.70	92.5	8.1
127	8186.78	3.5	4.2	139	8369.02	9.4	6.3	151	8456.88	71.9	6.1	163	8500.52	42.8	10.7
128	8218.56	3.6	4.3	140	8380.66	58.6	6.3	152	8458.64	38.5	5.8	164	8501.58	51.7	10.5
129	8222.20	4.3	4.2	141	8386.24	10.2	4.5	153	8468.09	33.1	7.3				

Table 8 Same as Table 7, but for the A_2 levels

i	E	$\langle A_\nu \rangle$	$\langle \rho \rangle$	i	E	$\langle A_\nu \rangle$	$\langle \rho \rangle$	i	E	$\langle A_\nu \rangle$	$\langle \rho \rangle$	i	E	$\langle A_\nu \rangle$	$\langle \rho \rangle$
88	7971.12	3.4	4.4	98	8222.04	3.5	4.4	108	8374.48	6.3	5.6	118	8461.92	54.0	6.1
89	7991.66	3.4	4.3	99	8239.07	3.5	4.5	109	8377.47	41.5	6.0	119	8466.82	61.6	7.8
90	8044.25	3.4	4.3	100	8267.05	3.4	4.5	110	8392.53	55.3	6.0	120	8473.02	95.8	7.0
91	8050.22	3.6	4.3	101	8275.09	2.8	5.4	111	8412.61	104.4	6.7	121	8479.92	87.6	7.5
92	8074.05	3.4	4.3	102	8297.50	3.2	5.0	112	8417.49	21.3	6.5	122	8485.17	7.4	4.6
93	8089.25	3.6	4.4	103	8323.84	3.2	5.5	113	8422.14	3.5	4.2	123	8489.37	74.5	8.2
94	8093.56	3.5	4.3	104	8346.84	5.5	5.7	114	8435.27	40.8	6.8	124	8492.39	84.0	8.5
95	8117.55	3.4	4.4	105	8360.18	4.4	4.4	115	8441.99	54.6	6.7	125	8494.66	79.9	7.5
96	8169.10	3.4	4.3	106	8361.94	8.2	5.4	116	8446.12	109.8	6.8	126	8498.52	46.8	11.0
97	8178.60	3.6	4.4	107	8365.42	4.6	4.7	117	8455.25	23.3	5.8	127	8502.41	44.5	12.0

Table 9 Same as Table 7 but for the E vibrational levels

i	E	$\langle A_\nu \rangle$	$\langle \rho \rangle$	i	E	$\langle A_\nu \rangle$	$\langle \rho \rangle$	i	E	$\langle A_\nu \rangle$	$\langle \rho \rangle$	i	E	$\langle A_\nu \rangle$	$\langle \rho \rangle$
294	7957.31	4.1	4.2	314	8218.56	3.6	4.3	334	8365.07	3.5	4.6	354	8450.02	26.5	6.5
295	7970.67	3.5	4.3	315	8222.11	3.5	4.4	335	8370.70	13.6	5.9	355	8452.12	48.4	5.7
296	7971.20	3.4	4.4	316	8222.20	4.3	4.2	336	8374.36	8.2	6.0	356	8456.32	27.6	5.5
297	7991.74	3.4	4.3	317	8238.75	3.4	4.3	337	8377.28	35.6	5.7	357	8456.85	85.1	6.5
298	8031.57	3.7	4.3	318	8239.32	3.5	4.5	338	8380.74	58.9	6.3	358	8459.02	26.9	5.8
299	8043.32	3.7	4.3	319	8244.94	3.3	4.6	339	8386.27	10.2	4.5	359	8461.18	47.2	6.2
300	8044.31	3.3	4.3	320	8267.12	3.4	4.5	340	8392.28	55.9	6.0	360	8466.87	61.2	7.8
301	8050.25	3.6	4.3	321	8273.86	3.1	5.2	341	8407.02	100.9	6.4	361	8468.51	37.9	7.4
302	8056.37	3.5	4.3	322	8275.17	2.8	5.4	342	8408.51	21.3	6.7	362	8473.23	91.7	6.8
303	8074.07	3.4	4.3	323	8285.43	3.4	4.3	343	8412.38	86.2	6.6	363	8473.59	90.2	7.1
304	8081.19	3.5	4.3	324	8289.81	3.1	5.1	344	8414.12	29.2	6.7	364	8477.05	47.4	5.9
305	8089.27	3.6	4.4	325	8297.65	3.2	5.0	345	8418.58	21.9	6.3	365	8480.17	11.7	7.7
306	8093.63	3.5	4.3	326	8318.95	3.3	5.0	346	8422.45	3.5	4.2	366	8481.14	65.4	7.0
307	8117.59	3.4	4.4	327	8323.81	3.2	5.5	347	8429.83	32.3	6.1	367	8483.12	57.6	6.8
308	8124.72	3.5	4.4	328	8332.03	3.6	5.4	348	8434.13	44.1	6.7	368	8485.42	9.4	4.5
309	8144.46	3.4	4.4	329	8346.77	5.5	5.7	349	8435.22	30.1	5.6	369	8489.18	69.1	7.8
310	8161.90	3.5	4.3	330	8354.20	4.9	4.7	350	8439.52	69.6	6.5	370	8489.67	73.8	8.2
311	8169.14	3.4	4.3	331	8356.30	8.5	5.8	351	8442.89	51.5	6.7	371	8490.71	43.1	8.9
312	8178.64	3.6	4.4	332	8359.93	5.5	5.0	352	8443.24	12.2	4.6	372	8492.48	82.0	8.5
313	8186.78	3.5	4.2	333	8360.74	5.4	5.0	353	8445.52	118.4	6.7	373	8493.40	48.8	6.7

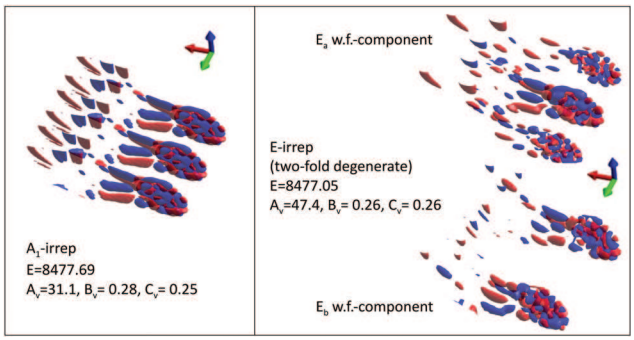

Fig. 10 Example of lifted A_1/E degeneracy for vibrational levels of $^{48}O_3$ ozone isotopomers due to the interaction between all three potential wells resulting to the splitting of ΔE = 0.64 cm^{-1} in rovibrational sub-band centers. The left-hand panel shows the totally symmetric A_1 function with the same amplitude in all three wells. The right-hand panel shows two components of the doubly degenerate wave functions of E symmetry of the S_3 group. Vibrational energies, E, and state-specific rotational constants A, B and C are given in cm^{-1}.

5 Conclusion

We have studied highly-excited rovibrational states of the main $^{48}O_3$ and ^{18}O-enriched $^{50}O_3$ isotopologues of ozone in a full-symmetry approach accounting for the three "open" potential wells. Bound state energies, wave functions, and expectation values for several characteristic quantities are computed in hyperspherical coordinates using the potential surface of ref. 5, which previously permitted an accurate description of metastable states[36] of O_3 as well as of the $^{16}O^{16}O + {}^{18}O \rightarrow {}^{16}O^{18}O + {}^{16}O$ isotopic exchange reactions.[55,56] A comparison of the present calculations with all available experimental data for the ozone band centers measured below 7950 cm^{-1} [4–6,9–15,59–61,66,68,69] gave the RMS (calculated/observed) deviation of about 1 cm^{-1}, which is significantly more accurate than other theoretical results that employed global three-wells methods. Predictions at such spectroscopic level of accuracy are expected to be helpful for analyses of future high-resolution observations at the experimentally yet unexplored energy range above 8000 cm^{-1} (that is >93% of the first O_2 + O dissociation threshold D_0).

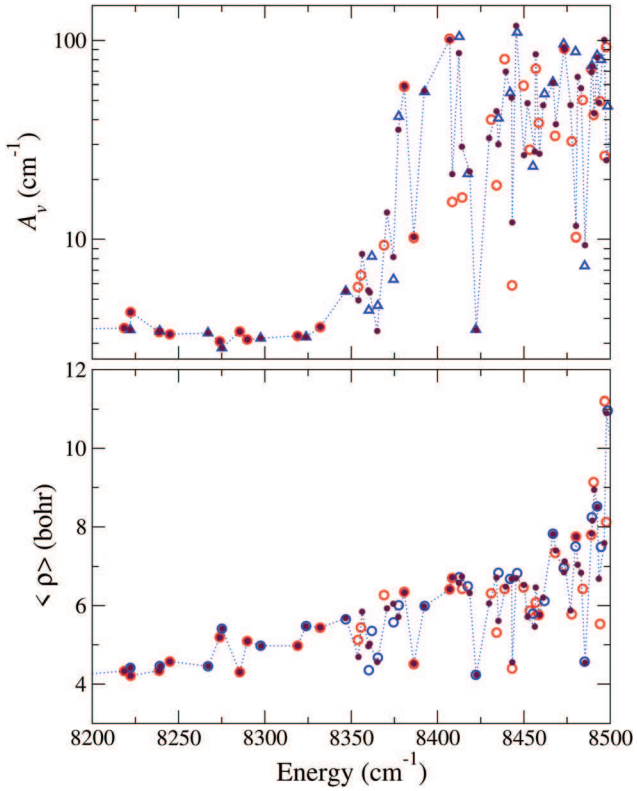

Fig. 11 Comparison of rotational constants $\langle A_\nu \rangle$ and averaged values of the hyper-radius of the vibrational levels of all three irreps of $^{48}O_3$: open circles correspond to A_1, open triangles to A_2, small closed circles to E. Only levels near the dissociation limit are shown, where the splitting due to tunneling is not negligible for certain levels.

The use of hyperspherical coordinates allowed us to account for permutation symmetry of the three or two identical nuclei of the $^{48}O_3$ and $^{50}O_3$ isotopologues. The main focus of the study was on the vibrational levels delocalized between the three potential wells of the ozone molecule because they determine the centers of observable rovibrational bands (even though some of the $J = 0$ levels are not spin allowed). The vibrational levels, corresponding to different irreps of the full permutation-inversion symmetry group and situated deep in the potential wells are three-fold or two-fold degenerate for the $^{48}O_3$ and $^{50}O_3$ isotopologues. With increasing energy towards the dissociation threshold, the vibrational parts of some wave functions come out of the wells, but not in a homogeneous way. Certain series of wave functions above 8000 cm^{-1} are still assignable as normal mode states (as shown in Fig. 12), remain localized in symmetric or asymmetric potential wells of $^{50}O_3$ (Fig. 3 and 4) and could be correctly calculated using the one-potential-well approximation. The importance of these series of levels (like those in Fig. 12) is that they are precursors of metastable scattering resonances that survive above D_0.

This is not the case of many other vibrational states as shown in Fig. 2, 5–7 and 10, where the wave functions are strongly delocalized, and the near degeneracy is lifted because of the interaction among potential wells. This occurs for the energies, for which classical periodic orbits[70] could not yet penetrate from one well to another. For this reason, we refer to this effect as to "tunneling splitting". Note that the situation here is more complicated than in the handbook example of ammonia-type tunneling, and this term has to be taken with caution. A direct tunneling between the ozone wells near the equilibrium is not feasible due to large barrier heights, which decrease rapidly as one of the bond-lengths is significantly stretched since the molecule reaches the plateau of the PES. The nodal patterns of the delocalized wave functions thus follow a curvi-linear large-amplitude path *via* the pre-dissociation plateau (Fig. 5–7). Finally, some partners of vibrational levels are not spin-allowed.

In practical terms this effect will result in a new type of perturbations in observable vibration–rotation bands: these bands will be split in sub-bands corresponding to A_1 and B_1 upper vibrational states of $^{50}O_3$ with shifted centers and different rotational constants as discussed in Sections 3.3 and 3.4. In the case of $^{48}O_3$, the splitting of sub-bands will correspond to A_1'/E' or to A_2'/E' upper state vibrations (Section 4.2). Another consequence is that the delocalized states of Fig. 6 and 7, corresponding to classical large amplitude "roaming" motion[64,65] of an O atom around an O_2 molecule, would be missing in the traditional one-well approximation.

We consider that our variational calculations are converged with respect to nuclear motion basis set to 0.01 cm^{-1} for $^{50}O_3$ and better than 0.01 cm^{-1} for $^{48}O_3$. All corresponding sub-band centers converged to this precision up to 99.5% of D_0 together with expectation values of rotational constants are given in the ESI.† We also supply the $\langle \phi \rangle$ value for each vibrational state of $^{50}O_3$, to distinguish where possible between symmetric 686 and asymmetric 668 wells or to detect the states where they are mixed.

The first practical conclusion is that these calculated data could guide the search of the bands in future analyses of very

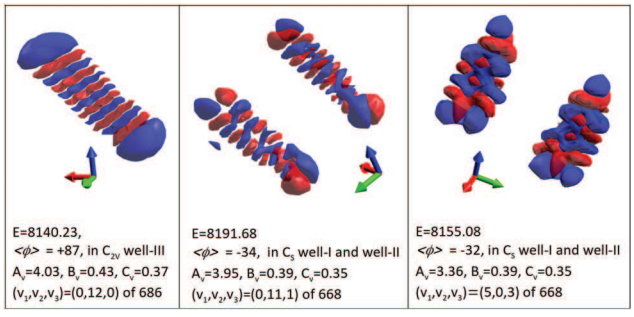

Fig. 12 Examples of some highly excited A-vibrational states of $^{50}O_3$ ozone isotopologues above 95% of D_0 with regular nodal structure, which remain assignable in terms of normal modes. Left-hand panel: wave function localized in the symmetric PES well-III assigned as (0,12,0) pure bending state of $^{16}O^{18}O^{16}O$. Central panel: wave function localized in two asymmetric wells assigned as combination state of $^{16}O^{16}O^{18}O/^{18}O^{16}O^{16}O$ with 11 bending quanta and 1 stretching quantum. Right-hand panel: wave function localized in two asymmetric wells assigned as combination state of $^{16}O^{16}O^{18}O/^{18}O^{16}O^{16}O$ with eight stretching quanta. Energies and expectation values of rotational constants A_ν, B_ν and C_ν are given in cm^{-1} and the averaged angle ϕ in degrees.

complicated experimental spectra near the dissociation threshold. The second one is that all empirical effective Hamiltonian models[4,8,11] (and references therein) which are traditionally employed for rovibrational spectra assignments will be no more valid at about 95% of D_0 and above. This is because the J-progressions and the sub-band centers will be different depending of the symmetry type of the upper vibrational state. The splitting values, which we provide in the present work, have to be accounted for in future effective empirical models. Even more critical will be changes for the states where the basis state function of $^{50}O_3$ vibrations are fully mixed among well-I, well-II and well-III as in Fig. 2 and 5–7. Traditional methods of spectra analyses and line assignments employed different models for the $^{16}O^{18}O^{16}O$ isotopomer and the $^{16}O^{16}O^{18}O$ isotopomer. In the first case, the C_{2v} point group model was used with only parallel bands for odd $\Delta\nu_3$ or only perpendicular bands for even $\Delta\nu_3$. In the second case, the C_s point group model was used with hybrid bands. It will no longer be possible to distinguish between two isotopomers for the energies where the scatter of $\langle\phi\rangle$ values and of $\langle r_{66}\rangle$ values occur in Fig. 2. The full permutation-inversion symmetry approach to $^{50}O_3$ spectra analyses considering both $^{16}O^{18}O^{16}O$ and $^{16}O^{16}O^{18}O$ isotopomers on equal footing will be mandatory in these cases.

Finally, we note that at energies very close to the dissociation limit to $O_2(X^3\Sigma_g^-) + O(^3P_2)$ the effect of non-adiabatic coupling and spin–orbit coupling must be included, since as many as 27 electronic states dissociate to this limit.[71,72] Furthermore, there are four conical intersections.[47] A correct description of the potential energy surfaces in this region may by obtained by diabatisation,[35,73–75] which would account for geometrical phase effects, and where the effect of spin–orbit coupling may be included as suggested recently by Guan and Yarkony.[76] We plan to account for these improvements in the theory with more thorough modeling towards the dissociation limit in a future work. However, it is unlikely that this would significantly change the main results of the present study concerning the effects of the band splitting due to interactions among potential wells, at least at the qualitative level. Note that very recent highly sensitive laser spectroscopic experiments[77] have confirmed our predictions for the new observed band centers of $^{48}O_3$ near 8000 cm^{-1} with the (obs.–calc.) accuracy of 1 to 2 cm^{-1}. Another challenge for experimental work would be more accurate measurements of the dissociation Do energy for the ozone isotopologues by spectroscopic methods similarly to the pump–probe results obtained for the water molecule.[78]

Conflicts of interest

There are no conflicts to declare.

Acknowledgements

This work was supported by the Russian Science Foundation Grant No. 19-12-00171 and the US National Science Foundation, Grant No. PHY-1806915. Supercomputer time was provided by the ROMEO HPC Centre at the University of Reims Champagne-Ardenne and by CRIANN (Centre Régional Informatique et d'Applications Numériques de Normandie). Q3

Notes and references

1 P. Fabian and M. Dameris, *Ozone in the Atmosphere*, Springer, 2014.
2 A. K. Smith, V. L. Harvey, M. G. Mlynczak, B. Funke, M. García-Comas, M. Hervig, M. Kaufmann, E. Kyrölä, M. López-Puertas, I. McDade, C. E. Randall, J. M. Russell III, P. E. Sheese, M. Shiotani, W. R. Skinner, M. Suzuki and K. A. Walker, *J. Geophys. Res.: Atmos.*, 2013, **118**, 5803–5821.
3 L. Hu, D. J. Jacob, X. Liu, Y. Zhang, L. Zhang, P. S. Kim, M. P. Sulprizio and R. M. Yantosca, *Atmos. Environ.*, 2017, **167**, 323–334.
4 A. Barbe, S. Mikhailenko, E. Starikova, M.-R. D. Backer, V. Tyuterev, D. Mondelain, S. Kassi, A. Campargue, C. Janssen, S. Tashkun, R. Kochanov, R. Gamache and J. Orphal, *J. Quant. Spectrosc. Radiat. Transfer*, 2013, **130**, 172–190.
5 V. G. Tyuterev, R. V. Kochanov, S. A. Tashkun, F. Holka and P. G. Szalay, *J. Chem. Phys.*, 2013, **139**, 134307.
6 V. G. Tyuterev, R. V. Kochanov and S. A. Tashkun, *J. Chem. Phys.*, 2017, **146**, 064304.
7 V. G. Tyuterev, A. Barbe, D. Jacquemart, C. Janssen, S. N. Mikhailenko and E. N. Starikova, *J. Chem. Phys.*, 2019, **150**, 184303.
8 J. M. Flaud and R. Bacis, *Spectrochim. Acta, Part A*, 1998, **54**, 3–16.
9 A. Campargue, S. Kassi, D. Romanini, A. Barbe, M.-R. De Backer-Barilly and V. G. Tyuterev, *J. Mol. Spectrosc.*, 2006, **240**, 1–13.
10 A. Campargue, A. Barbe, M.-R. De Backer-Barilly, V. G. Tyuterev and S. Kassi, *Phys. Chem. Chem. Phys.*, 2008, **10**, 2925–2946.
11 Y. L. Babikov, S. N. Mikhailenko, A. Barbe and V. G. Tyuterev, *J. Quant. Spectrosc. Radiat. Transfer*, 2014, **145**, 169–196.
12 E. Starikova, A. Barbe, M.-R. De Backer, V. G. Tyuterev, D. Mondelain, S. Kassi and A. Campargue, *J. Quant. Spectrosc. Radiat. Transfer*, 2014, **149**, 211–218.
13 A. Campargue, S. Kassi, D. Mondelain, A. Barbe, E. Starikova, M.-R. De Backer and V. G. Tyuterev, *J. Quant. Spectrosc. Radiat. Transfer*, 2015, **152**, 84–93.
14 E. Starikova, A. Barbe and V. G. Tyuterev, *J. Quant. Spectrosc. Radiat. Transfer*, 2019, **232**, 87–92.
15 S. Mikhailenko and A. Barbe, *J. Quant. Spectrosc. Radiat. Transfer*, 2020, **244**, 106823.
16 D. Mondelain, R. Jost, S. Kassi, R. H. Judge, V. Tyuterev and A. Campargue, *J. Quant. Spectrosc. Radiat. Transfer*, 2012, **113**, 840–849.
17 M. Kaufmann, S. Gil-López, M. López-Puertas, B. Funke, M. García-Comas, N. Glatthor, U. Grabowski, M. Höpfner,

G. P. Stiller, T. von Clarmann, M. E. Koukouli, L. Hoffmann and M. Riese, *J. Atmos. Sol.-Terr. Phys.*, 2006, **68**, 202–212.

18 A. G. Feofilov and A. A. Kutepov, *Surv. Geophys.*, 2012, **33**, 1231–1280.

19 K. Luther, K. Oum and J. Troe, *Phys. Chem. Chem. Phys.*, 2005, **7**, 2764–2770.

20 R. Schinke, S. Y. Grebenshchikov, M. Ivanov and P. Fleurat-Lessard, *Annu. Rev. Phys. Chem.*, 2006, **57**, 625–661.

21 T. Xie and J. M. Bowman, *Chem. Phys. Lett.*, 2005, **412**, 131–134.

22 R. A. Marcus, *Proc. Natl. Acad. Sci. U. S. A.*, 2013, **110**, 17703–17707.

23 A. Teplukhin and D. Babikov, *Faraday Discuss.*, 2018, **212**, 259–280.

24 D. Krankowsky and K. Mauersberger, *Science*, 1996, **274**, 1324–1325.

25 M. H. Thiemens and J. E. Heidenreich, *Science*, 1983, **219**, 1073–1075.

26 Y. Q. Gao and R. Marcus, *Science*, 2001, **293**, 259–263.

27 C. Janssen, J. Guenther, D. Krankowsky and K. Mauersberger, *Chem. Phys. Lett.*, 2003, **367**, 34–38.

28 K. Mauersberger, D. Krankowsky, C. Janssen and R. Schinke, *Adv. At., Mol., Opt. Phys.*, 2005, **50**, 1–54.

29 M. H. Thiemens, *Annu. Rev. Earth Planet. Sci.*, 2006, **34**, 217–262.

30 B. R. Johnson, *J. Chem. Phys.*, 1983, **79**, 1916.

31 V. Kokoouline and F. Masnou-Seeuws, *Phys. Rev. A: At., Mol., Opt. Phys.*, 2006, **73**, 012702.

32 J. Blandon, V. Kokoouline and F. Masnou-Seeuws, *Phys. Rev. A: At., Mol., Opt. Phys.*, 2007, **75**, 042508.

33 J. Blandon and V. Kokoouline, *Phys. Rev. Lett.*, 2009, **102**, 143002.

34 A. Alijah, *J. Mol. Spectrosc.*, 2010, **264**, 111–119.

35 A. Alijah and V. Kokoouline, *Chem. Phys.*, 2015, **460**, 43.

36 D. Lapierre, A. Alijah, R. Kochanov, V. Kokoouline and V. Tyuterev, *Phys. Rev. A*, 2016, **94**, 042514.

37 A. Banichevich, S. D. Peyerimhoff and F. Grein, *Chem. Phys.*, 1993, **178**, 155–188.

38 R. Siebert, R. Schinke and M. Bittererová, *Phys. Chem. Chem. Phys.*, 2001, **3**, 1795–1798.

39 R. Siebert, P. Fleurat-Lessard, R. Schinke, M. Bittererová and S. Farantos, *J. Chem. Phys.*, 2002, **116**, 9749–9767.

40 M. Ayouz and D. Babikov, *J. Chem. Phys.*, 2013, **138**, 164311.

41 F. Holka, P. G. Szalay, T. Müller and V. G. Tyuterev, *J. Phys. Chem. A*, 2010, **114**, 9927–9935.

42 R. Dawes, P. Lolur, J. Ma and H. Guo, *J. Chem. Phys.*, 2011, **135**, 081102.

43 M. Lepers, B. Bussery-Honvault and O. Dulieu, *J. Chem. Phys.*, 2012, **137**, 234305.

44 R. Dawes, P. Lolur, A. Li, B. Jiang and H. Guo, *J. Chem. Phys.*, 2013, **139**, 201103.

45 D. J. Tannor, *J. Am. Chem. Soc.*, 1989, **111**, 2772–2776.

46 P. García-Fernandez, I. B. Bersuker and J. E. Boggs, *Phys. Rev. Lett.*, 2006, **96**, 163005.

47 A. Alijah, D. Lapierre and V. Tyuterev, *Mol. Phys.*, 2018, **116**, 2660–2670.

48 R. Schinke and P. Fleurat-Lessard, *J. Chem. Phys.*, 2004, **121**, 5789–5793.

49 V. G. Tyuterev, R. Kochanov, A. Campargue, S. Kassi, D. Mondelain, A. Barbe, E. Starikova, M. R. De Backer, P. G. Szalay and S. Tashkun, *Phys. Rev. Lett.*, 2014, **113**, 143002.

50 S. Ndengué, R. Dawes, X.-G. Wang, T. Carrington Jr, Z. Sun and H. Guo, *J. Chem. Phys.*, 2016, **144**, 074302.

51 A. Teplukhin and D. Babikov, *Phys. Chem. Chem. Phys.*, 2016, **18**, 19194–19206.

52 C. Petty, R. F. K. Spada, F. B. C. Machado and B. Poirier, *J. Chem. Phys.*, 2018, **149**, 024307.

53 I. Gayday, A. Teplukhin and D. Babikov, *J. Chem. Phys.*, 2019, **150**, 101104.

54 I. Gayday, A. Teplukhin, B. K. Kendrick and D. Babikov, *J. Chem. Phys.*, 2020, **152**, 144104.

55 P. Honvault, G. Guillon, R. Kochanov and V. Tyuterev, *J. Chem. Phys.*, 2018, **149**, 214304.

56 C. H. Yuen, D. Lapierre, F. Gatti, V. Kokoouline and V. G. Tyuterev, *J. Phys. Chem. A*, 2019, **123**, 7733–7743.

57 B. Ruscic, Unpublished results obtained from active thermochemical tables (ATcT) based on the Core (Argonne), Thermochemical Network version 1.110, 2010. available at atct.anl.gov.

58 O. I. Tolstikhin, S. Watanabe and M. Matsuzawa, *J. Phys. B: At., Mol. Opt. Phys.*, 1996, **29**, L389.

59 C. Camy-Peyret, J.-M. Flaud, A. Perrin, V. Malathy Devi, C. P. Rinsland and M. A. H. Smith, *J. Mol. Spectrosc.*, 1986, **118**, 345–354.

60 J. M. Flaud, M. T. Bourgeois, A. Barbe, J. J. Plateaux and C. Camy-Peyret, *J. Mol. Spectrosc.*, 1994, **165**, 464–469.

61 A. Barbe, E. Starikova, M. R. De Backer and V. G. Tyuterev, *J. Quant. Spectrosc. Radiat. Transfer*, 2018, **218**, 231–247.

62 P. R. Bunker and P. Jensen, *Molecular Symmetry and Spectroscopy*, NRC Research Press, 1998.

63 G. W. King, R. M. Hainer and P. C. Cross, *J. Chem. Phys.*, 1943, **11**, 27–42.

64 J. M. Bowman, *Mol. Phys.*, 2014, **112**, 2516–2528.

65 F. A. L. Mauguière, P. Collins, Z. C. Kramer, B. K. Carpenter, G. S. Ezra, S. C. Farantos and S. Wiggins, *J. Chem. Phys.*, 2016, **144**, 054107.

66 M.-R. De Backer, A. Barbe, E. Starikova, V. G. Tyuterev, D. Mondelain, S. Kassi and A. Campargue, *J. Quant. Spectrosc. Radiat. Transfer*, 2013, **127**, 24–36.

67 A. Teplukhin and D. Babikov, *J. Chem. Phys.*, 2016, **145**, 114106.

68 D. Mondelain, A. Campargue, S. Kassi, A. Barbe, E. Starikova, M.-R. De Backer and V. G. Tyuterev, *J. Quant. Spectrosc. Radiat. Transfer*, 2013, **116**, 49–66.

69 E. Starikova, A. Barbe, D. Mondelain, S. Kassi, A. Campargue, M.-R. De Backer and V. G. Tyuterev, *J. Quant. Spectrosc. Radiat. Transfer*, 2013, **119**, 104–113.

70 O. V. Egorov, F. Mauguiere and V. G. Tyuterev, *Russ. Phys. J.*, 2020, 1–9.

71 P. Rosmus, P. Palmieri and R. Schinke, *J. Chem. Phys.*, 2002, **117**, 4871–4877.

72 M. Tashiro and R. Schinke, *J. Chem. Phys.*, 2003, **119**, 10186–10193.
73 W. Domcke and C. Woywod, *Chem. Phys. Lett.*, 1993, **216**, 362–368.
74 M. Baer and A. Alijah, *Chem. Phys. Lett.*, 2000, **319**, 489.
75 V. Dhindhwal, M. Baer and N. Sathyamurthy, *J. Phys. Chem. A*, 2016, **120**, 2999–3008.
76 Y. Guan and D. R. Yarkony, *J. Phys. Chem. Lett.*, 2020, **11**, 1848–1858.
77 S. Vasilchenko, A. A. Barbe, E. Starikova, S. Kassi, A. Campargue and D. Mondelain, private communication.
78 P. Maksyutenko, T. R. Rizzo and O. V. Boyarkin, *J. Chem. Phys.*, 2006, **125**, 181101.